remote sensing

MDPI

Article

Sea Storm Analysis: Evaluation of Multiannual Wave Parameters Retrieved from HF Radar and Wave Model

Simona Saviano [1,2,*,†], Anastasia Angela Biancardi [3,†], Marco Uttieri [2,4], Enrico Zambianchi [2,3], Luis Alberto Cusati [5], Andrea Pedroncini [5], Giorgio Contento [6,‡] and Daniela Cianelli [1,2]

1 Department of Research Infrastructures for Marine Biological Resources, Stazione Zoologica Anton Dohrn, Villa Comunale, 80121 Naples, Italy; daniela.cianelli@szn.it
2 CoNISMa—National Inter-University Consortium for Marine Sciences, Piazzale Flaminio, 00196 Rome, Italy; enrico.zambianchi@uniparthenope.it
3 Department of Science and Technologies, Parthenope University of Naples, Centro Direzionale Is.C4, 80143 Naples, Italy; anastasiaangela.biancardi@studenti.uniparthenope.it
4 Department of Integrative Marine Ecology, Stazione Zoologica Anton Dohrn, Villa Comunale, 80121 Naples, Italy; marco.uttieri@szn.it
5 DHI srl, 16149 Genova, Italy; lcu@dhigroup.com (L.A.C.); anp@dhigroup.com (A.P.)
6 Department of Naval Architecture, Ocean and Environmental Engineering, University of Trieste, 34127 Trieste, Italy; contento@units.it
* Correspondence: simona.saviano@szn.it
† These authors contributed equally to this work.
‡ Deceased before the submission of the paper.

Abstract: Intense atmospheric disturbances, which impact directly on the sea surface causing a significant increase in wave height and sometimes strong storm surges, have become increasingly frequent in recent years in the Mediterranean Sea, producing extreme concern in highly populated coastal areas, such as the Gulf of Naples (Western Mediterranean Sea, Central Tyrrhenian Sea). In this work, fifty-six months of wave parameters retrieved by an HF radar network are integrated with numerical outputs to analyze the seasonality of extreme events in the study area and to investigate the performance of HF radars while increasing their distances from the coast. The model employed is the MWM (Mediterranean Wind-Wave Model), providing a wind-wave dataset based on numerical models (the hindcast approach) and implemented in the study area with a 0.03° spatial resolution. The integration and comparison with the MWM dataset, carried out using wave parameters and spectral information, allowed us to analyze the availability and accuracy of HF sampling during the investigated period. The statistical comparisons highlight agreement between the model and the HF radars during episodes of sea storms. The results confirm the potential of HF radar systems as long-term monitoring observation platforms, and allow us to give further indications on the seasonality of sea storms under different meteorological conditions and on their energy content in semi-enclosed coastal areas, such as the Gulf of Naples.

Keywords: sea storm; HF radar; wave model; Gulf of Naples

Citation: Saviano, S.; Biancardi, A.A.; Uttieri, M.; Zambianchi, E.; Cusati, L.A.; Pedroncini, A.; Contento, G.; Cianelli, D. Sea Storm Analysis: Evaluation of Multiannual Wave Parameters Retrieved from HF Radar and Wave Model. *Remote Sens.* **2022**, *14*, 1696. https://doi.org/10.3390/rs14071696

Academic Editor: Silvia Piedracoba

Received: 28 February 2022
Accepted: 28 March 2022
Published: 31 March 2022

1. Introduction

Changes in atmospheric storms, as predicted for the upcoming years in the Mediterranean area, can induce alterations in water levels [1]. Sea storm events impact coastal areas, causing several problems, such as floodings, beach erosion and damages to structures. The seasonal distribution of sea storms, their management and the information given to coastal communities are of great importance, especially in today's changing climate scenario [2].

In the Mediterranean region, storm surges may have significant differences due to the storm characteristics and the topography of each area [3]. The Mediterranean wave models are now able to represent the complexity of the geomorphology of the region; recent

downscaling techniques have improved simulated trends using high spatial-resolution models, forced by high-resolution atmospheric fields [4].

In the last decade, High Frequency radars (HFrs) have been added to the instruments available for the study of wave fields [5–7], their wave data having been validated for different geographical areas and for different types of HFr systems (mostly, CODAR and WERA) [8–10]. Validation studies using in situ observations [11–14], satellite acquisitions [15,16] and model outputs [17–19] have yielded results that have proven the reliability of these systems.

HFrs allowing the synoptic observation of vast marine areas have been tested to analyze extreme events, proving to be useful tools for analyzing coastal storms in geographical areas characterized by energetically important events [20–22]. The identification of coastal storm thresholds is site-specific and depends on bathymetry, the exposure of a location to the winds and the local characteristics of the investigated coastal area [23]. In coastal storm analyses, the parameters considered are the main directions of storms and the storms' energies; moreover, mean, maximum or peak wave-height parameters are also used [24–27].

Among the Mediterranean sub-basins, the Tyrrhenian Sea (Western Mediterranean Sea) is characterized by a complex geomorphology and vast urbanized coastal areas that require careful monitoring in terms of wave fields and evolution of storm surges. The wave climate of the Tyrrhenian Sea varies strongly with the seasons, with low wave height (Hs; in the order of a few tens of centimeters) in summer replaced by waves up to and beyond 3 m during winter and autumn [28,29]. In the Gulf of Naples (GoN) (Central Tyrrhenian Sea), the presence of a network of HFrs allowed a near real-time monitoring of the wave field over several consecutive years [9,11,19]. A year-long comparison of the wave parameters (significant wave height, direction and period) between the HFr sites and a wave buoy deployed in the outer part of the basin was presented in [9], and in [11] a wave climatology of the study area was assessed to demonstrate the potential of an integrated platform for coastal studies.

In [19], a three-year characterization of the wave heights, periods and directions in the GoN was carried out by comparing HFr-derived wave parameters with WavewatchIII (WWIII) and Simulating Waves Nearshore (SWAN) model predictions. Skill metrics, intended as a set of statistical tools used to verify the robustness of the comparisons, indicated that the HFr measurements were in general good agreement with both the WWIII and SWAN measurements. In this work, we expand on these previous results by comparing and integrating HFr wave data with the outputs of the Mediterranean Wind-Wave Model (MWM), a wind-wave hindcast dataset for the Mediterranean Sea. The MWM, developed by the DHI (formerly, the Danish Hydraulic Institute) and the Hydrodynamics and MetOcean Laboratory (HyMOLab, University of Trieste), may now provide up to forty-two years of hourly data for the entire Mediterranean Sea, implementing a last-generation model chain at a very high spatial resolution [30].

We focus on fifty-six months of retrieval (May 2008–December 2012). The first part of the analysis is related to the comparison of the overall performance of and agreement between the MWM and HFr data; then, we analyze in more detail the extreme events recorded in the GoN using both wave parameters and spectra energy. The correlation between the HFr and MWM co-located data allowed us to evaluate the wave-model output in the GoN and its accuracy during storm events. The measuring skills and the ability to measure extreme wave events of the HFr systems at increasing distances from the coast are also assessed.

The paper is organized as follows. The study area is described in Section 2, along with datasets, the data-analysis methodology and a description of the validation metrics. The results over the observation period are shown in Section 3, and the corresponding discussion is presented in Section 4.

2. Materials and Methods

2.1. Study Area

The GoN (Figure 1; Central Tyrrhenian Sea) is characterized by a complex geomorphology [31] and mixed carbonate–siliciclastic systems [32]. The basin communicates with the open Tyrrhenian Sea through the "Bocca Grande" (opening between Capri and Ischia Islands). The coastal area of the GoN is particularly sensitive to extreme events owing to the presence of urban settlements, commercial activities, infrastructures and submerged archeological sites [33–35].

Previous studies on the analysis and identification of the wave field in this area and its variation during the seasons were based on temporal series collected at HFr sites validated with in situ acquisitions [9], compared with wave model outputs [19] and used in multi-platform wave analyses [11]. Results showed good agreement between measurements recorded by the different platforms, depicting recurrent patterns characterized by a strong seasonal variability. In the GoN, the wave field is strongly dependent on the meteorological conditions of the Tyrrhenian area [9,36], with a wintertime low-pressure system linked to the North Atlantic cyclone, and on the local winds influenced by the reliefs surrounding the GoN. In winter, the most frequent winds blow from N-NE and NE directions, alternating with S-SW winds associated with low-pressure systems [37]. In summer, the reinforcement of the Azores anticyclone and, in recent years, of the African anticyclone [38] leads to long periods of stable high atmospheric pressure. This determines a wind regime driven by breezes, with winds from SW and NE alternating over the day. Depending on the local orography and bottom topography, as well as on exposures to different geographical sectors, the main wave directions change as a function of the considered sub-basin [9,11].

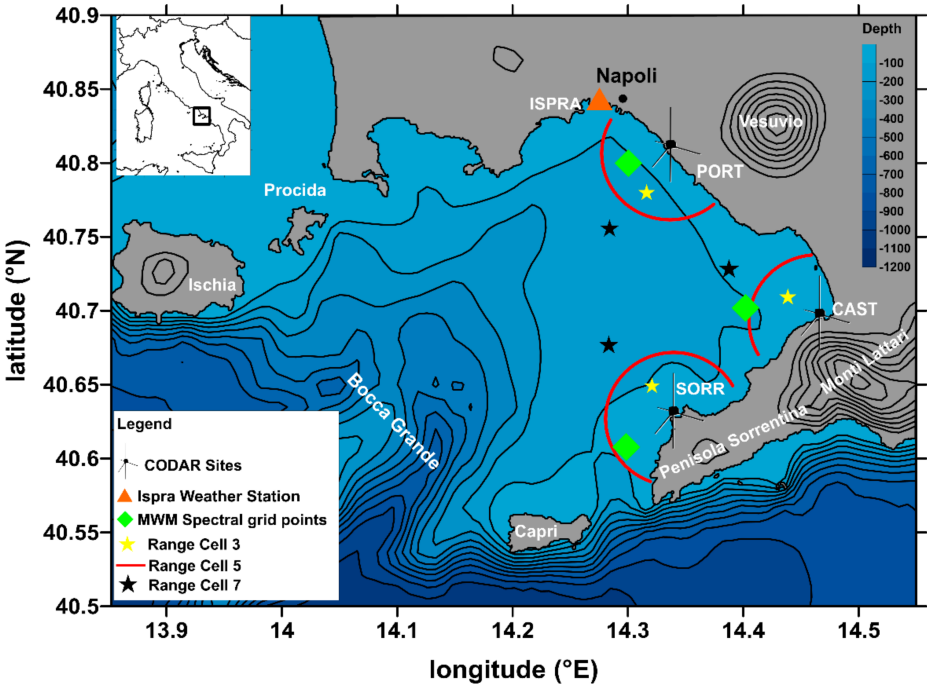

Figure 1. Map of the Gulf of Naples (Central Tyrrhenian Sea) with the locations of the three HF radar sites (antennas), ISPRA weather station (orange triangle) and the MWM model grid points of spectral data (green diamonds). The red semi-circles represent Range Cell 5 (RC5) of acquisitions, yellow stars represent Range Cell 3 (RC3) and black stars represent Range Cell 7 (RC7) offshore distances, respectively (see text). The bathymetric contours are spaced every 100 m; the orographic ones are spaced every 300 m. Coastline data: NOAA National Geophysical Data Center; Coastline extracted: WLC (World Coast Line); Date retrieved: 1 April 2015; http://www.ngdc.noaa.gov/mgg/shorelines/shorelines.html, accessed on 8 September 2011; bathymetric and orographic data from [39].

2.2. HF Radar Wave Observations

HFr wave parameters have been collected by direction-finding CODAR SeaSonde HFr systems (Figure 1). The three short-range HFrs, deployed between 2004 and 2008, use 25 MHz as working frequency [36] and cover different sub-sectors of the GoN (PORT, CAST and SORR; Figure 1). This system has been used in the GoN to analyze the characteristics of the surface current [40–42] and wave fields [9,11,19], as well as to retrieve information on wind direction data [43].

In SeaSonde systems, the wave parameters—significant wave height (Hs), centroid period (T_{HF}) and direction (θ_{HF})—are extracted from the second-order spectrum by applying the Pierson–Moskowitz model [44]. It has been verified on numerous occasions that this model is robust enough to describe the unimodal energy spectrum and the wave field [6,45]. In this work, the wave parameters were measured and averaged along range cells (RCs) centered on each antenna and regularly spaced by 1 km. For each cell, a single spatially averaged RC value was provided for each wave parameter. In the GoN, wave measurements were performed on 12 range cells for the PORT and SORR sites and over 15 range cells for CAST using the proprietary CODAR software (SeaSonde Radial Suite R7u2). Individual spectra were recorded and averaged every ten minutes, calculating the average of four spectra falling within the given time window [44]. The homogeneity of the ocean spectra was assumed over each HFr RC [6,9,20,44].

2.3. Mediterranean Wave Model (MWM)

The MWM is a model-derived dataset of hourly wave and wind parameters starting from 01 January 1979, and obtained from a latest-generation chain of models. The models and datasets used for the development of the MWM database are: the Climate Forecast System Reanalysis (CFSR) global reanalysis dataset, produced and freely published by the National Centers for Environmental Prediction (NCEP) [45], and hourly (re-forecast) data with a space resolution of 0.5°. These data are used as initial conditions (IC) and boundary conditions (BC) of the WRF-ARW (Weather Research and Forecasting-Advanced Research WRF) atmospheric model (version 3.4.1) developed by National Center for Atmospheric Research (NCAR) [46–48].

WRF-ARW model is presently considered among the best state-of-the-art, non-hydrostatic meteorological models; it is supported by a worldwide community that contributes to its local use and development (http://www.mmm.ucar.edu/wrf/OnLineTutorial/index.htm, accessed on 1 May 2020; http://www.wrf-model.org/index.php, accessed on 1 May 2020).

2.4. MIKE 21 Spectral Waves (SW)

The MIKE 21 Spectral Waves (SW) model, developed by DHI [49], has been used in thousands of offshore and coastal applications worldwide [50,51]. In the following paragraphs, a brief description of the MIKE 21 SW model is given (for more information, see [52]), with specific interest in the implementation adopted by MWM.

MIKE 21 SW is a third-generation spectral wind-wave model simulating the growth, decay and transformation of waves generated by wind and storm surges in offshore and coastal areas. It can be divided into two different formulations. The first is a directional decoupled parametric formulation based on parameterization of the wave-action conservation equations and made in the frequency domain. The second is a fully spectral formulation based on wave-action conservation equations as described in, e.g., [53,54], where the directional-frequency wave-action spectrum is a dependent variable.

The discretization of the governing equation in the geographical and spectral space is performed using the cell-centered finite-volume method. In the geographical domain, an unstructured mesh technique is used. Time integration is performed using a fractional-step approach with which a multi-sequence explicit method is applied for the propagation of a wave action. The fully spectral formulation has been adopted for the production of the MWM database. The time integration of the governing equations is dynamically determined in order to verify the stability criteria. The only driving force is represented

by the two components of wind fields $U10$ and $V10$, which represent, respectively, the x and y wind components at the elevation of 10 m. In order to generate waves, the wind transfers energy into the water body through a process of decoupled air–sea interaction. The spectral discretization used in the wave model guarantees a high level of accuracy with a reasonable computational effort. The model domain covers the entire Mediterranean Sea with a spatial resolution of around 0.1° in offshore areas, while in coastal areas or in areas where the depth is less than 100 m, the spatial resolution increases up to about 0.03°. The wave model is forced by the wind fields obtained from the WRF atmospheric model [55].

The wave model generates results in terms of wave parameters (wave height (Hs_m), peak period (Tp_m), mean period (Tm_m), wave direction (θ_m), etc.) over the whole domain. In addition, the model also stores hourly spectral parameters—in terms of wave energy as a function of direction and frequency—in predefined output locations.

The bathymetry data derives from the GEBCO_08 database, which considers a 30 arc-second grid of global elevations and is a continuous terrain model for ocean and land [56]. GEBCO scatter data have been used for only offshore areas with depths of up to 500 m, while for shallow water areas, the model uses the dataset of nautical charts available in Database CM93/3 of CMAP [57].

One of the key parameters for wave models is the "spectral resolution" given by discrete frequencies and directions. This parameter should be high enough to correctly represent the "real shape" of the wave spectrum, but it should also guarantee acceptable computational times and memory consumptions. In terms of frequency range, the minimum frequency f_{min} that corresponds to the maximum wave period T_{max}, according to the relation $f = 1/T$, should be able to capture the longest wave periods that can occur in the Mediterranean Sea. Analyzed ordinary and extreme waves highlight that almost all the wave energy connected to waves in the Mediterranean Sea is associated with a wave period of between 1.5 and 20 s [58].

A logarithmic distribution for discrete frequencies was considered because the wave periods are concentrated below 8–10 s in the Mediterranean Sea [58]; thus, a number of frequencies of around 30 is considered to be adequate for a proper discretization of wave energy spectra in this area. The following formulation was therefore used:

$$f_j = f_0 \cdot c^n \quad (1)$$

where f_j is the frequency; f_0 is the minimum frequency (=0.04); c is the frequency factor (=1.1 as default) and n is the number of frequencies, ranging from 0 to 29 because 30 is the total number of frequencies [52].

The discrete frequency ranges from 0.04 Hz to 0.63 Hz. The choice of the number of discrete directions is also the result of investigations and tests; in particular, numerous tests were carried out, each of which was characterized by a different spatial resolution. The outcomes of a large number of tests suggested that, considering 24 directions, a very good compromise between accuracy of results and computational time may be obtained. The computational time dependent on the wave model is linearly dependent on the number of discrete directions. Since the wave directions vary in a 360° rose, the directional resolution of the wave model is 360°/24 = 15°.

2.5. Wind Data

In situ wind observations collected by a weather station managed by ISPRA (Istituto Superiore per la Protezione e la Ricerca Ambientale), located in the port of Naples (Molo del Carmine; latitude: 40.840N; longitude: 14.275E; anemometric sensor height: 10 m AMSL; data freely downloadable at http://www.mareografico.it/; access date: 19 May 2021; Figure 1) were used in the extreme event analysis. The station was equipped with wind speed (SIAP + MICROS, mod. T006 TVV) and direction (SIAP + MICROS, mod.T007 TDV) transducers and with a barometric sensor (SIAP + MICROS, mod. PA9880). Hourly averaged data were used in the study. Wind speed and direction are closely related to the

evolution of extreme events, so wind data during storm events are analyzed to identify the wind jet that generates sea storms.

2.6. Data Analysis Methods

A comparison between HFr and MWM wave measurements was drawn along different RCs to assess the retrieval of extreme events from offshore zones to the coast. HFr wave parameters from RC3, RC5 and RC7 (i.e., 3, 5 and 7 km from the antenna, respectively) were analyzed in comparison to those obtained at co-located sites by using the SW model. As in previous works [9,11,19,43], RC5 was considered a benchmark RC, trading off between distance from the coast (ensuring enough echo intensity) and depth (avoiding wave breaking). Instead, RC3 and RC7 were used to assess the robustness of HFr retrieval in areas nearer to (RC3) and farther from (RC7) the antenna.

The following statistics were used in the analysis:

$$\rho = \frac{1}{N} \frac{\sum_i^N (S_i - \overline{S})(O_i - \overline{O})}{\sigma_O \sigma_S} \tag{2}$$

$$NRMSE = \sqrt{\frac{\sum_i^N (S_i - O_i)^2}{\sum O_i^2}} \tag{3}$$

$$NBIAS = \frac{\overline{S} - \overline{O}}{\overline{O}} \tag{4}$$

$$HH = \sqrt{\frac{\sum_i^N (S_i - O_i)^2}{\sum S_i O_i}} \tag{5}$$

where S_i and O_i are simulated (MWM) and observed (HFr) data, respectively, whereas the overbar indicates the average. ρ represents the correlation index, spanning in the ± 1 range, where +1 (-1) indicates perfect correlation (anti-correlation) for two investigated series, while 0 indicates total lack of it. σ stands for the data standard deviation.

NRMSE (Normalized Root Mean Square Error) is a measure of the distance between two datasets and is one of the most employed indexes for evaluating the goodness of fit between the observed values of a variable and the corresponding values predicted by a model.

NBIAS is a measure of the average component of the error, which should result in close-to-0 values for series in good agreement. The Hanna and Heinold index proposed by [59], referred to as *HH*, was employed. *HH* allows one to overcome drawbacks that may arise from negatively biased measurements, i.e. that underestimate measured quantities, as suggested by [60].

The irregular nature of the wind causes irregular wind waves with different heights, periods and directions. For this reason, wind waves are usually described using spectral techniques, with which the random movement of the sea surface is treated as the sum of the components of the wave harmonics. In particular, we considered the energy density E (f, θ), which represents the quantity of energy stored in a given system as a function of the frequency (f) and direction (θ) of the waves; it represents the variance of the elevation of the free surface and can be defined as follows [61]:

$$E = \int_{f_{low}}^{f_{high}} \int_0^{2\pi} \mathrm{E}(\mathrm{f},\ \theta)\ \mathrm{df}\ \mathrm{d}\theta \tag{6}$$

The SW database uses a fully spectral formulation; consequently, the energy density of the input spectrum must be the normal energy density E (f, q), where f is the relative frequency and q is the direction of the wave expressed in m^2 s/rad.

Directional spreading, also known as directional standard deviation (DSD), is defined in MIKE 21 as follows:

$$DSD = \sqrt{2\left(1 - \sqrt{a^2 + b^2}\right)} \tag{7}$$

$$a = \frac{1}{m_0} \int_0^{2\pi} \int_0^n \cos(\theta) E(\sigma, \theta) d\sigma \, d\theta \tag{8}$$

$$b = \frac{1}{m_0} \int_0^{2\pi} \int_0^n \sin(\theta) E(\sigma, \theta) d\sigma \, d\theta \tag{9}$$

where m_0 is zero-th moment and n is the directional spreading index.

In order to identify storm events in the analyzed HFr dataset, we considered an Hs threshold of 1.25 m recorded over a period of longer than six hours [9,11]. Sea storms with inter-event separations of thirty-six hours and wave heights less than 1 m were considered as single events [24].

The coastal storm energy (E) was estimated for each event by using an alternative formulation of Equation (6), as proposed by [24], where $t1$ and $t2$ denote the beginning and the end of an event, respectively:

$$\mathrm{E} = \int_{t1}^{t2} Hs^2 dt \tag{10}$$

3. Results

3.1. Model and HFr Preliminary Assessment

A qualitative analysis of the significant wave heights during the different seasons was carried out to compare the patterns of the retrieved data and to assess the differences under different weather conditions.

Figures 2–4 show the Hs time series for the HFr (in blue) and MWM (in red) for the SORR, CAST and PORT sites, respectively; the right panels show the scatter plots of Hs on the RC and MWM for each site. As already evidenced in previous works [9,11,19], the GoN HFr system captured wave data more efficiently during the autumn/winter period, which was characterized by more intense conditions than in the spring/summer period, when the onset of the breeze regime is associated with Hs values below detectability (0.5 m). The extended dataset analyzed in the present work confirmed this pattern, as is evident from the time series shown in Figures 2–4.

Subsequently, the skill metrics listed in the previous section (ρ, *NBIAS*, *NRMSE* and *HH* index) were applied to compare the wave heights retrieved from the two platforms. The good agreement shown in (Figures 2–4, right panels) at a multiannual scale was confirmed by the skill metrics computed for the yearly comparisons (Table 1). The statistical values of ρ, *NBIAS*, *NRMSE* and *HH* index were calculated for each radar site over the three range cells identified in the previous section (RC3, RC5 and RC7) over the years. Generally, the ρ value was robust for RC5 and RC7 in each site with values > 0.5; the *NRMSE* was low, between 0.01 and 0.06; the *NBIAS* was negative and the *HH* index showed values between 0.29 and 0.93. The PORT site skill metrics showed the best agreement between the HFrs and the SW model, with ρ values from 0.57 to 0.85 during the analyzed time series and the lowest values for the *NBIAS* and *HH*. At CAST, the skill metrics were in line with previous studies for RC5 and RC7 with ρ values from 0.5 to 0.77. From RC3, ρ scored the lowest values, with a minimum in 2010 of 0.28. This result might have been due to the position of the CAST site as well as to the intricate bathymetry of the area. In addition, the skill metrics for the year 2011 from RC3 were not calculated due to recurrent failures of the CAST antenna and a lower retrieval in this RC.

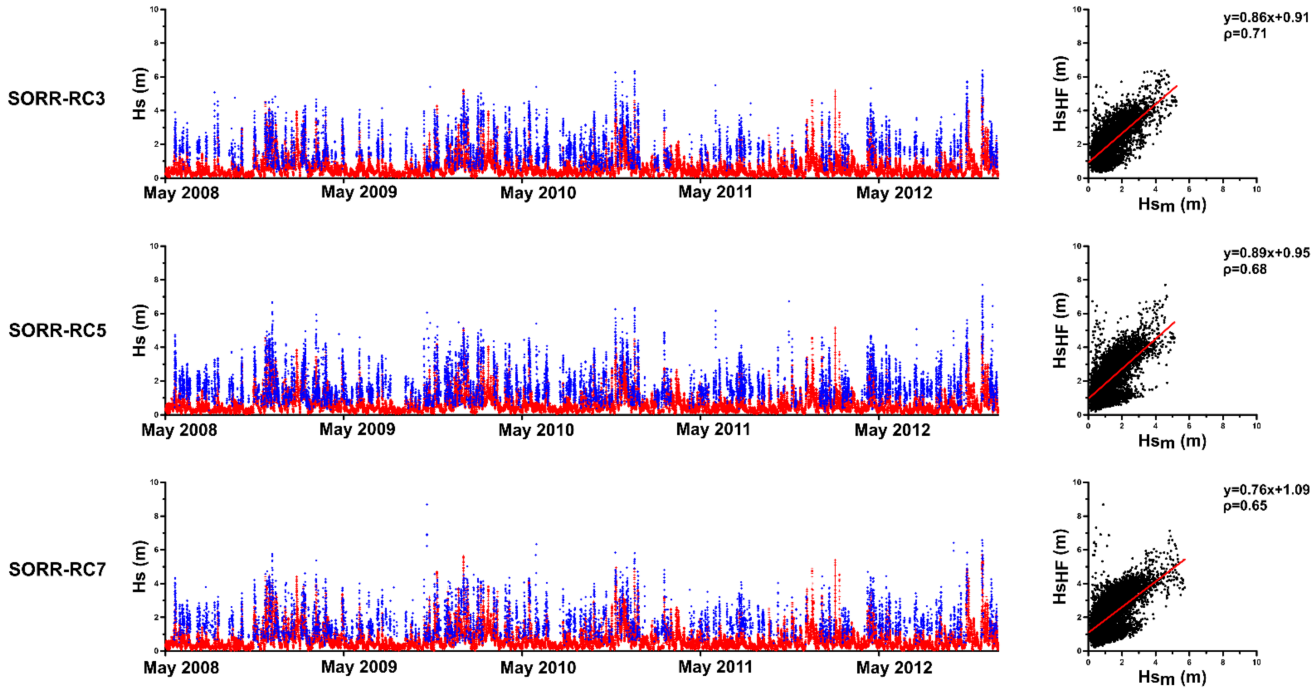

Figure 2. (**left**) Time series comparison of wave heights (Hs) between SORR HFr (blue) and MWM (red) from RC3, RC5 and RC7 (upper, middle and lower panel, respectively). (**right**) Scatter plots of Hs values recorded by the HFr and retrieved by using the MWM model at the three RCs.

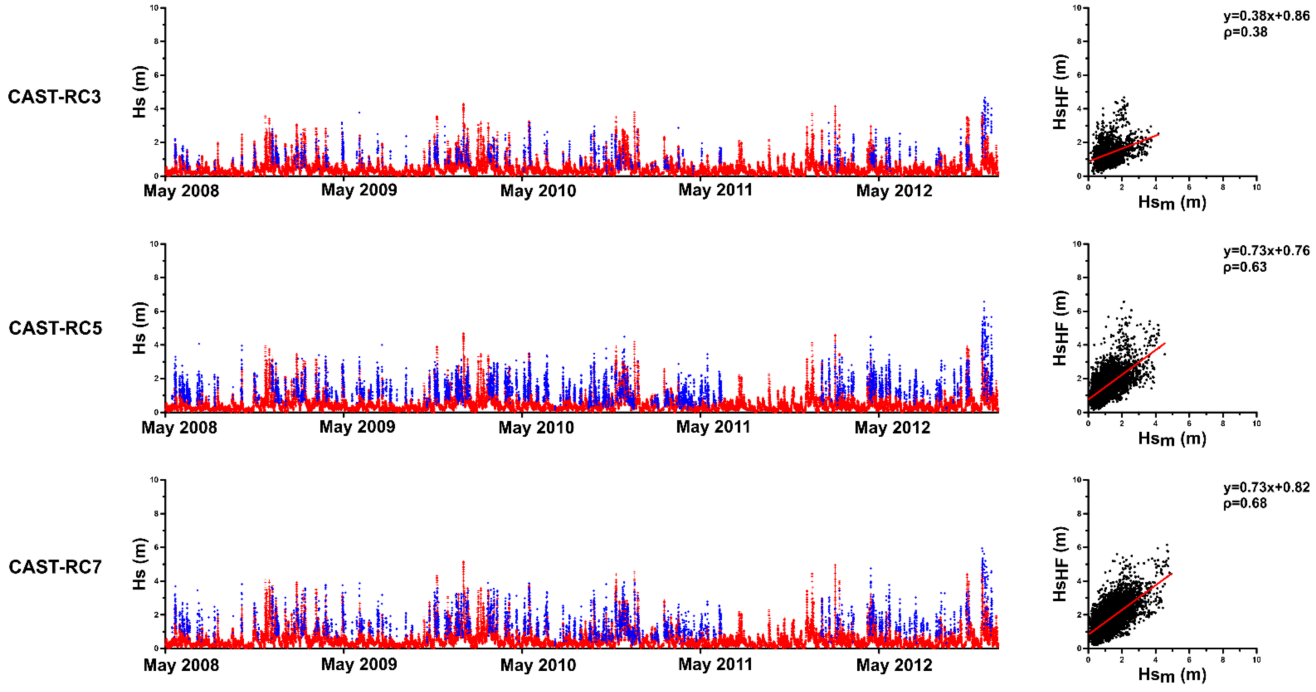

Figure 3. (**left**) Time series comparison of wave heights (Hs) between CAST HFr (blue) and MWM (red) from RC3, RC5 and RC7 (upper, middle and lower panel, respectively). (**right**) Scatter plots of Hs values recorded by the HFr and retrieved by using the MWM model at the three RCs.

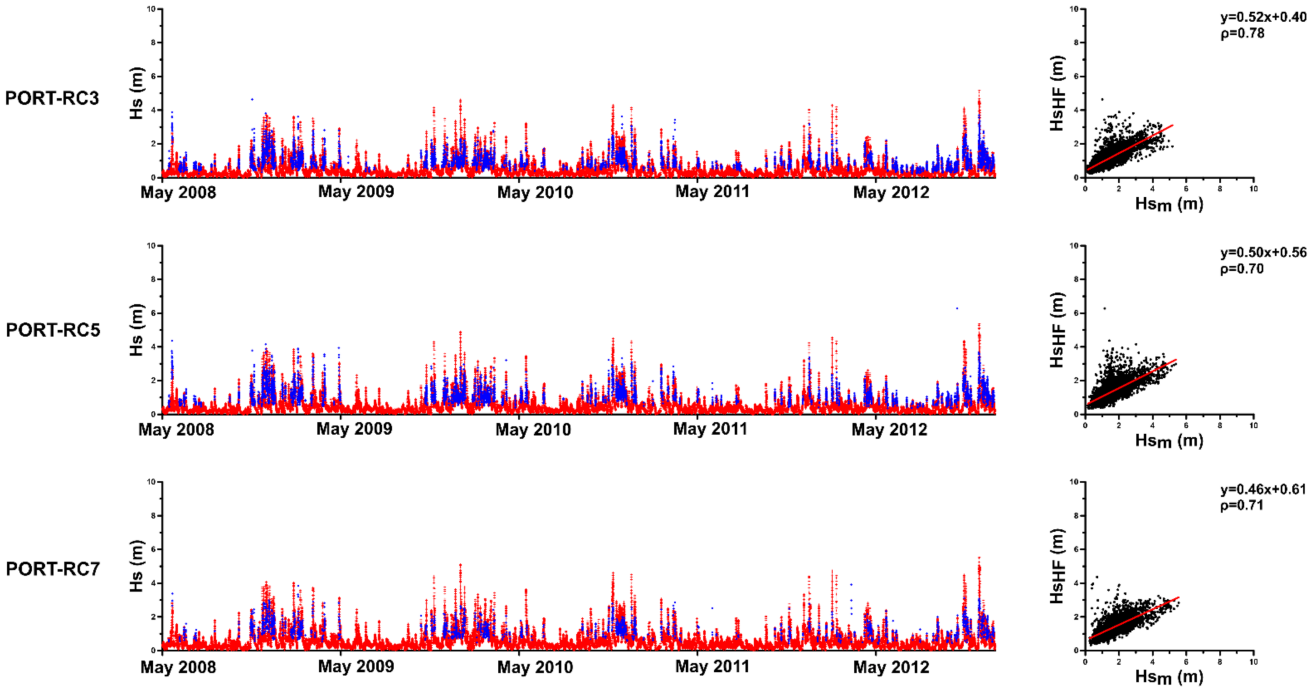

Figure 4. (**left**) Time series comparison of wave heights (Hs) between PORT HFr (blue) and MWM (red) from RC3, RC5 and RC7 (upper, middle and lower panel, respectively). (**right**) Scatter plots of Hs values recorded by the HFr and retrieved by using the MWM model at the three RCs.

Table 1. Skill metrics of the comparison between Hs in three RCs (RC3, RC 5 and RC7) and MWM (co-located data) during the period analysis (May 2008–December 2012).

Year	Site	ρ	*NRMSE*	*NBIAS*	*HH*
2008	SORR-RC3	0.61	0.02	−0.70	0.55
	SORR-RC5	0.61	0.01	−0.69	0.67
	SORR-RC7	0.64	0.01	−0.67	0.63
	CAST-RC3	0.75	0.02	−0.67	0.29
	CAST-RC5	0.56	0.02	−0.68	0.55
	CAST-RC7	0.64	0.02	−0.70	0.54
	PORT-RC3	0.78	0.01	−0.61	0.37
	PORT-RC5	0.7	0.02	−0.67	0.36
	PORT-RC7	0.76	0.02	−0.65	0.33
2009	SORR-RC3	0.66	0.01	−0.64	0.51
	SORR-RC5	0.64	0.01	−0.61	0.65
	SORR-RC7	0.58	0.01	−0.60	0.66
	CAST-RC3	0.29	0.02	−0.65	0.48
	CAST-RC5	0.49	0.01	−0.64	0.54
	CAST-RC7	0.6	0.01	−0.65	0.56
	PORT-RC3	0.66	0.01	−0.52	0.44
	PORT-RC5	0.57	0.02	−0.57	0.4
	PORT-RC7	0.62	0.03	−0.54	0.39
2010	SORR-RC3	0.77	0.01	−0.63	0.63
	SORR-RC5	0.73	0.01	−0.61	0.63
	SORR-RC7	0.7	0.01	−0.60	0.62
	CAST-RC3	0.28	0.02	−0.56	0.55
	CAST-RC5	0.63	0.01	−0.56	0.55
	CAST-RC7	0.71	0.01	−0.57	0.47
	PORT-RC3	0.8	0.01	−0.43	0.42
	PORT-RC5	0.71	0.02	−0.49	0.4
	PORT-RC7	0.74	0.03	−0.45	0.4

Table 1. *Cont.*

Year	Site	ρ	*NRMSE*	*NBIAS*	*HH*
2011	SORR-RC3	0.46	0.02	−0.68	0.8
	SORR-RC5	0.5	0.02	−0.66	0.92
	SORR-RC7	0.44	0.02	−0.66	0.93
	CAST-RC3	-	-	-	-
	CAST-RC5	0.39	0.02	−0.60	0.73
	CAST-RC7	0.36	0.02	−0.62	0.65
	PORT-RC3	0.69	0.01	−0.57	0.8
	PORT-RC5	0.77	0.04	−0.66	0.36
	PORT-RC7	0.62	0.06	−0.60	0.4
2012	SORR-RC3	0.79	0.01	−0.69	0.56
	SORR-RC5	0.75	0.01	−0.65	0.73
	SORR-RC7	0.71	0.01	−0.65	0.72
	CAST-RC3	0.38	0.03	−0.71	0.64
	CAST-RC5	0.7	0.01	−0.73	0.63
	CAST-RC7	0.77	0.01	−0.70	0.59
	PORT-RC3	0.85	0.01	−0.49	0.38
	PORT-RC5	0.77	0.03	−0.57	0.4
	PORT-RC7	0.75	0.03	−0.55	0.42

A comparison of the SORR site data shows ρ values from 0.58 to 0.79, a lower *NRMSE* error and a lower *HH*, except for 2011, which represented the worst performance in comparative terms for SORR, with ρ from 0.44 to 0.5 and a high value of the *HH* index.

For the same site, similar values of each skill-metric parameter were found in the different range cells, demonstrating that when the antenna worked correctly the quality of the data did not change between the offshore area and the coastal one, although a difference remained in the data acquired in RC3 for problems related to shallow water (see Table S1, Supplementary Materials).

3.2. Extreme Events Analysis

The list of the sea storm events detected on the three RCs over the investigated time window is reported in the Supplementary Materials (Table S2). The highest number of events (37) was recorded in 2010, while 2011 was the year that reported the lowest number of records (7 events). The sea storms were mainly characterized by winds from the S-SW, which was as expected considering the geomorphology of the basin; occasionally, some events were associated with NE wind.

The analysis of wave direction (data not shown) highlighted a site-dependent pattern, confirming what was reported in previous works [9,11,19]. The sector of wave provenance was relatively constant over the seasons for each HFr station due to the geomorphological configuration of the GoN. In autumn and winter, stronger winds resulted in higher Hs_{HF} values with the dominant wave directions between 180° and 210° for PORT, 265° and 275° for CAST and 270° and 300° for SORR [9,11,19].

According to the storm classification presented in [24] based on the storm energy (E) value, most of the events listed in the Supplementary Materials were categorized as class I (weak), with an average duration of about 25 h. For the CAST and SORR locations, some events were categorized as class II (moderate) and class III (significant), while only a few events in the SORR acquisition dataset were classified as class IV (severe). The class V storm category was represented by a single event retrieved from SORR. The event had a total duration of 79 h (information from the bulletin of Campania Region Civil Protection); unfortunately, SORR Hs_{HF} and wind acquisitions were interrupted around 60 h and 30 h, respectively. These results are consistent with previous observations evidencing the most energetic storms in the SORR sector due to the associated fetch and wind regime in the area [11,19,36]. For a given HFr site, E was higher along RC5 and RC7 and decreased along

RC3, changing the storm class, especially for the innermost sites (CAST and PORT; see Supplementary Materials).

In Figure 5, the averaged parameters of Hs_m, T_{HF}, E and duration from RC5 for storm classes are shown. As can be observed, the increase in storm category was accompanied by an increase in all wave variables. The wave period was the variable showing the smallest variation with storm category, with maximum recorded T_{HF} values of about 13 s.

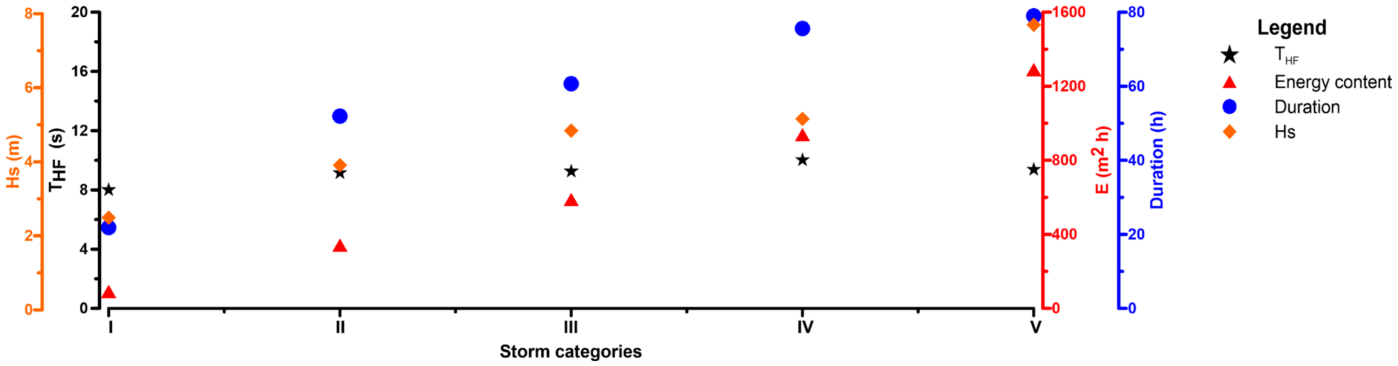

Figure 5. Class-averaged values of wave storms retrieved from RC5 of SeaSonde network in the GoN.

In the following paragraphs, a detailed analysis of a selection of sea storm events is presented, focusing the attention on those events retrieved by all three HFrs on all the RCs used in the analysis. Some acquisitions may have been lost due to temporary failures of the station. The characteristics of each event are shown in Table 2.

Table 2. Main parameters of sea storms selected.

Event Date	Duration (h)	Mean Wind Direction (°)	Mean Wind Velocity (m/s)	E SORR (m^2h)	E CAST (m^2h)	E PORT (m^2h)
04 December 2008–07 December 2008	81	200.8	5.6	1180	265.8	102.4
01 January 2009–03 January 2009	50	202.5	4.5	120.9	42.2	46.8
08 November 2010–10 November 2010	68	211.3	9.5	597.8	117.7	317.9
28 November 2012–30 November 2012	63	188.8	13.3	1290	812.1	422.6

Figures 6–9 show the evolution of the events selected to describe the storms in the GoN typical of the winter and autumn seasons retrieved on RC5. To analyze the energy content in different areas of the GoN, three grid points of the SW model located near the RC5 of each radar site (taken as benchmarks for HFr measurements; see Figure 1, green diamonds) were used to obtain the spectral data at the onset and conclusion of each storm. The first and third panels of each event analysis (Figures 6–9) show the model spectral energy when the wind jet starts and finishes, respectively. The central panels illustrate the evolution, during the event, of the wind intensity (in green), Hs_m (in red), Hs_{HF} (in black) and directional spreading (blue). All the times are in GMT.

The selected storms were all driven by S-SW wind. It could have been that each storm was seen late by the innermost antennas of the network and with different wave characteristics in terms of Hs and E content. The wind jet of the first event (Figure 6) started on 04 December 2008 at 14:00 (15 h) with a wind speed of 2.7 m/s; it increased until the wind reached its maximum speed (16.3 m/s) on 05 December 2008 at 18:00 (43 h). Observing the central figures, we can notice that in correspondence with the maximum wind speed, the maximum Hs_{HF} for SORR (6.6 m) was recorded, while the maximum Hs_m was shifted by six hours with a value of 3.6 m.

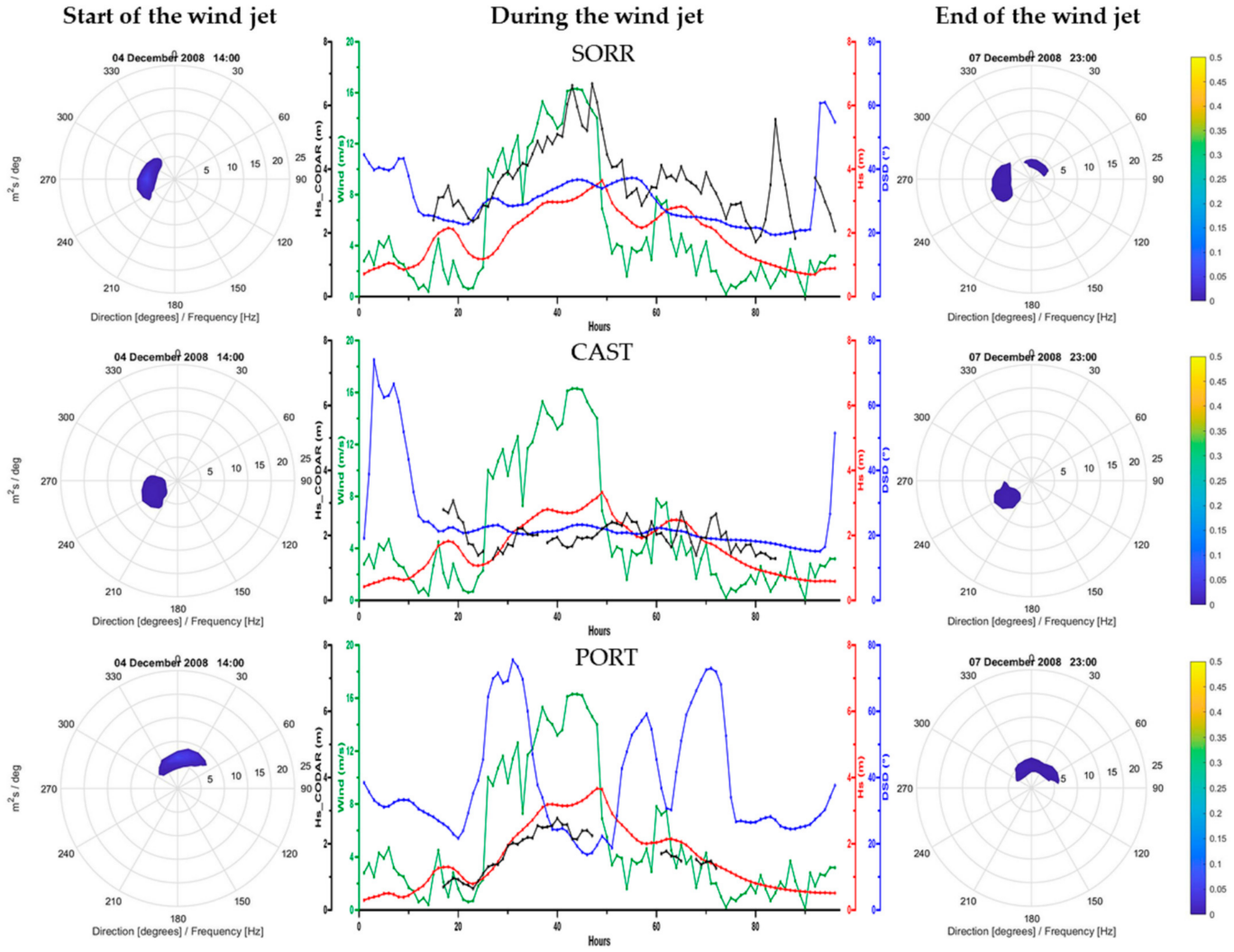

Figure 6. Evolution of the storm event recorded on 4–7 December 2008. The first and third panels show the model spectral energy as the wind jet started and finished, respectively. The central panels illustrate the evolution, during the event, of the wind intensity (in green), significant wave height (of the model Hs_m (in red) and retrieved by the HFr Hs_{HF} (in black)) and directional spreading DSD (blue).

For the CAST site, the event was seen before it was seen at the SORR site (04 December 2008 at 16:00 (17 h)) with 2.8 m for the Hs_{HF} while the model Hs_m was 3.3 m on 06 December 2008 at 00:00 (49 h). Finally, the maximum Hs value of the PORT site was recorded three hours earlier than at the SORR site with a value of 2.8 m, while the maximum value recorded by the model was one hour earlier than the other sites with a value of 3.6 m.

The model underestimated the values recorded by the Hs_{HF} for the SORR site, while it overestimated the Hs data for the other sites.

Starting from 07 December 2008 at 17:00 (90 h), the wind dropped and rotated from the SW toward the northern quadrants; finally, the event ended on 07 December 2008 at 23:00 (96 h) with a NE wind.

Comparing the hourly plot of the energy density with the DSD trend (Figure 6), we can see that the highest energy density values for the SORR and CAST sites were recorded from 05 December 2008 at 07:00 (32 h) to 06 December 2008 at 03:00 (52 h) and from 05 December 2008 at 04:00 (29 h) to 06 December 2008 at 06:00 (55 h; see the spectral plots in Supplementary Materials, Figure S1), respectively; this corresponded to an almost constant trend of the DSD in correspondence with high values of Hs. On the contrary, for PORT, the

event was not particularly intense, and this can be seen from the fluctuating curve of the DSD and low values of Hs.

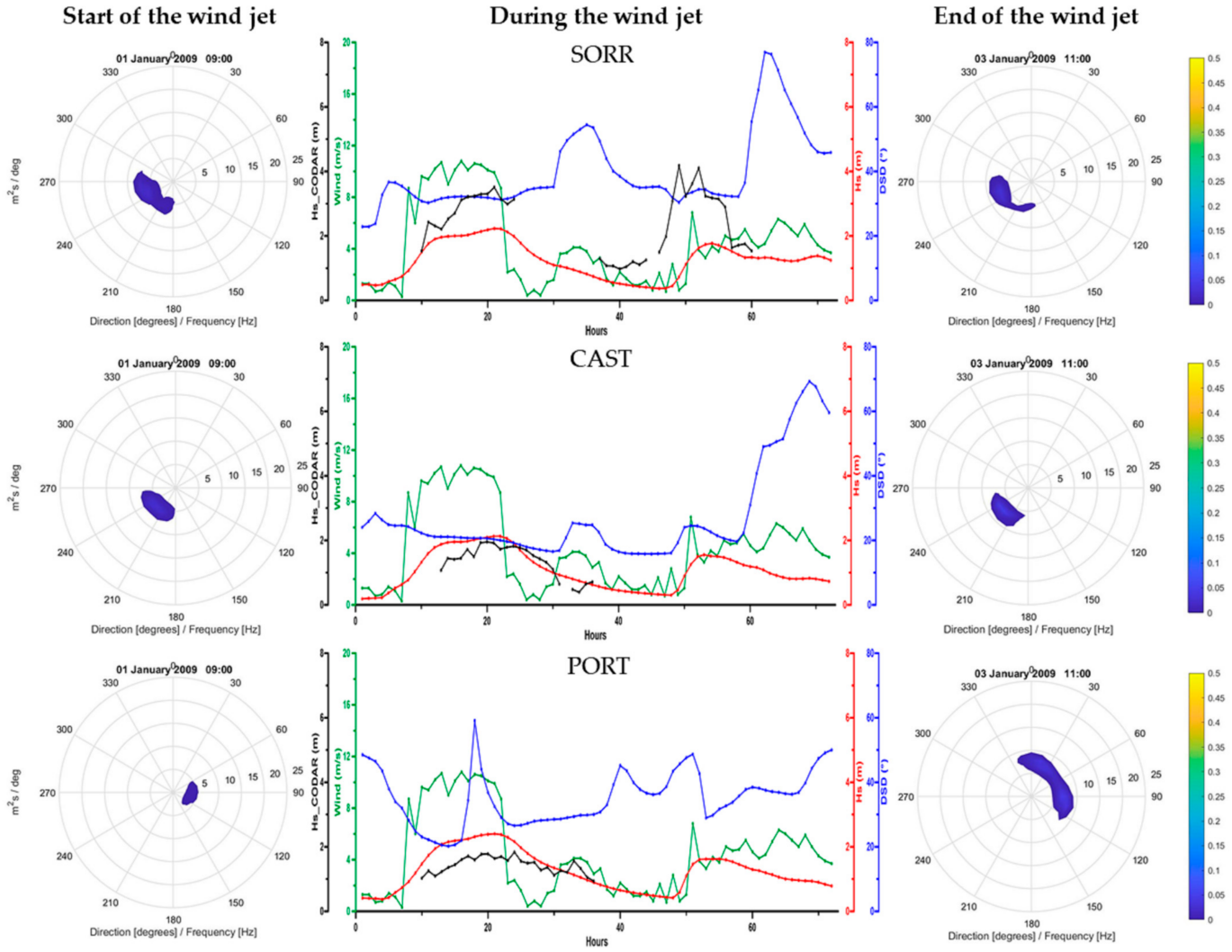

Figure 7. Evolution of storm event (January 2009). First and third panels show the model spectral energy at the wind jet starts and finishes, respectively. The central panels illustrate the evolution, during the event, of the wind intensity (in green), significant wave height (of the model (in red) and retrieved by the HFr Hs_{HF} (in black)) and the directional spreading DSD (blue).

The second analyzed event (Figure 7) started on 1 January 2009 with a wind speed of about 10 m/s from 09:00 (10 h) to 20:00 (21 h). The SORR and CAST sites reached maximum Hs_{HF}s of 3.5 m (on 01 January 2009 at 20:00 (21 h)) and 1.9 m (on 1 January 2009 19:00 (20 h)), respectively. Instead, PORT reached a maximum energy density later (1 January 2009 at 23:00 (24 h)) with a value of 1.8 m. Moreover, in this case, the Hs_m from the model underestimated the wave heights observed by the radar at the SORR site and overestimated them at CAST and PORT.

Starting from 2 January 2009 at 01:00 (26 h), the wind rotated toward the N and decreased in intensity, but the HFrs did not record data during this period. The radar acquisition started again at only SORR, when the wind blew again from the S on 3 January 2009 01:00 (50 h), scoring a second peak (4 m) at 03:00 (52 h) after a wind speed of 6.8 m/s. The event ended on 03 January 2009 at 11:00 (60 h).

However, the output of the model (density energy) showed that the event was seen at SORR from 1 January 2009 at 10:00 (11 h) to 2 January 2009 at 03:00 (28 h), and a second peak was seen on 3 January 2009 from 04:00 (53 h) to 11:00 (60 h). CAST was most intense

from 1 January 2009 at 10:00 (11 h) to 2 January 2009 at 03:00 (28 h). A very weak event was registered for PORT from 3 January 2009 at 07:00 (56 h) to 23:00 (72 h). (See the spectral plots in Supplementary Materials, Figure S2).

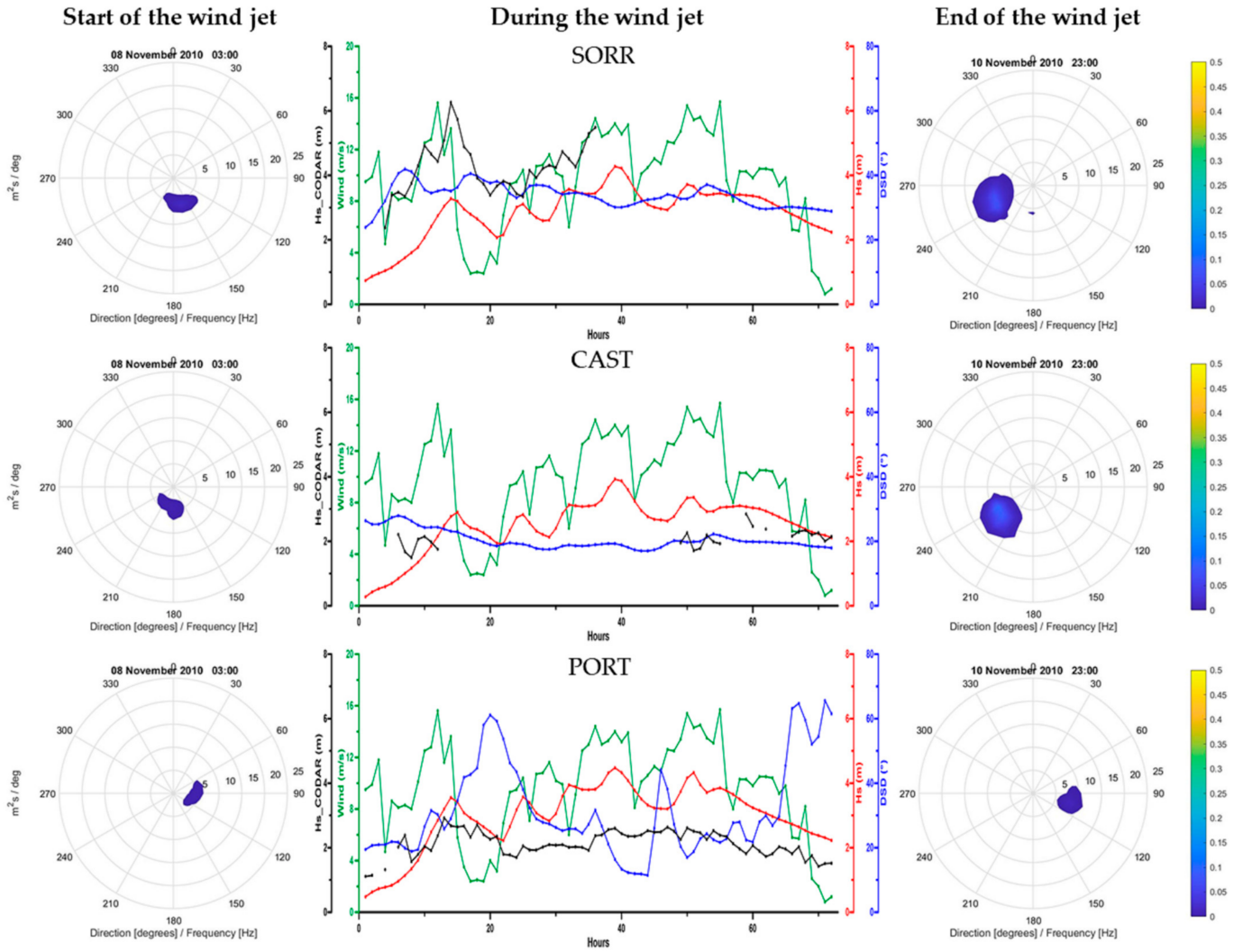

Figure 8. Evolution of storm event (November 2010). First and third panels show the model spectral energy at the wind jet starts and finishes, respectively. The central panels illustrate the evolution, during the event, of the wind intensity (in green), significant wave height (of the model (in red) and retrieved by the HFr Hs_{HF} (in black)) and the directional spreading DSD (blue).

Comparing the DSD with the energy density observations, it can be seen that for the SORR and CAST sites, the highest energy density values are identified when the DSD curve assumes an almost constant trend and the Hs curve assumes values high in the same range. Observing the hourly energy densities, it can be inferred that the PORT event was not very intense, and this can also be confirmed by the lower values of Hs and a non-constant trend of the DSD.

The event recorded on 8 November 2010 (Figure 8) commenced at 03:00 (4 h) with a wind speed of 4.7 m/s and grew rapidly to exceed 10 m/s with a peak of 15.6 m/s at 11:00 (12 h). The wind decreased and then increased again until reaching its maximum speed on 10 November 2010 at 06:00 (55 h) of 15.7 m/s. The wind then decreased in speed until reaching its minimum value on 10 November 2010 at 22:00 (71 h) of 0.8 m/s. The event ended on 10 November 2010 at 23:00 (72 h).

Although the radars did not work very well for the SORR and CAST sites, we can observe that the SORR radar followed the trend of the wind even if it reached its maximum

speed two hours later (14 h; 6 m). The model showed the same trend of the radar even if it was underestimating the values (2.7 m compared to the 6 m of the radar). For CAST, the acquisitions were missing due to the malfunction of the structure.

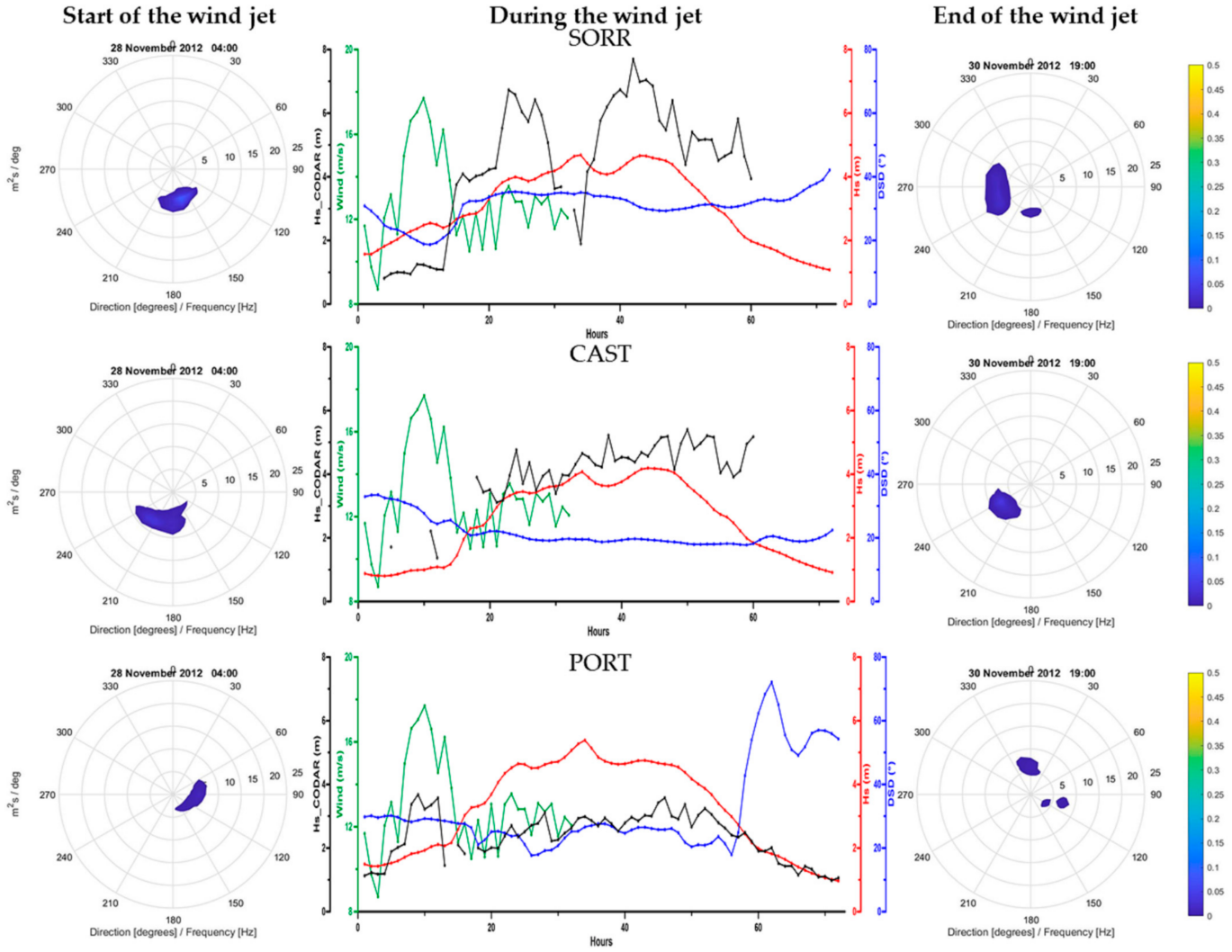

Figure 9. Evolution of storm event (November 2012). Left and right panels show the model spectral energy at the wind jet starts and finishes, respectively. The central panels illustrate the evolution, during the event, of the wind intensity (in green), significant wave height (of the model (in red) and retrieved by the HFr Hs_{HF} (in black)) and directional spreading DSD (blue).

PORT was characterized by a less intense event than the other sites since the wind coming from the SW is partially blocked by the Sorrento peninsula and the island of Capri. Comparing the red curve with the black one, it can be seen that the model reproduces the trend of the event but overestimates the radar values.

Comparing the DSD with the hourly energy-density graphs, almost constant values of DSD and high values of Hs corresponding to a large variation in energy density are manifested, as they are for the previous event. In fact, variations in energy density are found for SORR from 08 November 2010 at 10:00 (11 h) until 10 November 2010 at 21:00 (70 h), but the maximum values range from 08 November 2010 at 10:00 (11 h) to 16:00 (17 h), from 9 November 2010 at 00:00 (25 h) until 20:00 (45 h) and from 10 November 2010 at 06:00 (55 h) to 16:00 (65 h), when the DSD curve tends to assume constant values. A similar characterization of the event is found for CAST from 8 November 2010 at 13:00 (14 h) until 10 November 2010 at 22:00 (71 h; see the spectral plots in Supplementary Materials,

Figure S3). PORT, however, reported a very variable DSD throughout the event, and no large variations in energy density were found.

The last event (Figure 9) was the only event categorized as a V class. It began on 28 November 2012 at 04:00 (5 h) with a wind speed of 13.1 m/s. The maximum recorded wind speed was 17.7 m/s, found on 28 November 2012 at 9:00 (10 h), after which the wind started to be more or less constant with a speed of around 12 m/s. The acquisition stopped on 29 November 2012 at 08:00 (33 h) due to a malfunction of the weather station. The event ended on 30 November 2012 at 19:00 (68 h).

Starting from 28 November 2012 at 18:00 (19 h), SORR tallied Hs_{HF} values higher than 4 m until reaching the maximum of 7.7 m at 17:00 on 29 November 2012 (42 h). CAST, however, began to show values exceeding 4 m starting from 28 November 2012 at 23:00 (24 h) until reaching the maximum of 5 m on 29 November 2012 at 22:00 (47 h). PORT never presented Hs_{HF} values higher than 4 m, but starting from 07:00 on 28 November 2012 (8 h), the wave height exceeded 3 m until 11:00 (12 h), reaching its maximum value of 3.6 m. Moreover, for this event, the model underestimated the HFr observations for SORR and CAST while overestimating Hs compared to PORT.

Observing the hourly energy density graphs, we can notice that for the SORR site, the event scored the maximum values on 29 November 2012 at 02:00 (27 h) until 23:00 (48 h); instead, CAST reached the highest values on 28 November 2012 at 16:00 (17 h) until 30 November 2012 at 05:00 (54 h). Instead, PORT showed lower energy density values than the other two sites in agreement with the recorded wave height values, starting from 15:00 on 28 November 2012 (16 h) until 29 November 2012 at 04:00 (29 h; see the spectral plots in Supplementary Materials, Figure S4). These values also correspond in this case to an almost constant DSD parameter and high values of Hs in the same interval.

4. Discussion

Today, HFr systems are used worldwide [62,63] as efficient instruments for simultaneously measuring and monitoring surface currents [23–25,64] and wave parameters [9,65–69]. In this study, we analyzed a fifty-six-month long wave-data time series, recorded by SeaSonde HFr systems installed in the GoN, with a special focus on sea storms. In particular, the seasonality of the sea storms and the evolution of the wave field from offshore to coastal areas were analyzed, comparing HFr data with the SW model dataset on three RCs for each station of the network.

Studies on extreme events have assessed the reliability of HFr systems [20–22,70]. In particular, the results presented in [70] proved that a synergistic observational and modeling approach can provide a comprehensive characterization of severe wave conditions in coastal areas, merging the benefits of the complementary natures of both systems. HFr wave parameters can also be assimilated in wave models [71,72], solving local dynamics mainly in intricate geographical areas.

The analysis presented here on the comparison between HFr data and model outputs in the GoN shows an agreement between the two platforms, confirming that HFrs are valid tools for monitoring the wave fields in coastal areas. The skill parameters revealed an overall good agreement in the Hs retrieved by the HFrs and MWM, with matching time series patterns in line with previous results from the same basin but using other models [19] and with other studies in different areas [12,17,21]. This confirms the robustness of radar measurements, independent of the numerical platform used for the comparison. Some considerations are noteworthy in regards to the RCs. For the PORT and SORR sites, ρ attained similar values over the three investigated RCs, pointing to a similar performance of the radars at increasing distances from the coast. At CAST, however, the ρ scores for RC3 are remarkably lower than the ones for RC5 and RC7, with the only exception of 2008. This may suggest that the geomorphology of the area covered by the CAST radar may present specific features hampering proper wave acquisitions at short distances from the coast, while the RCs located farther offshore may nonetheless return robust wave measurements. These features may also explain the reduced percentage of data acquired in comparison

to RC5 and RC7. These results are in line with previous studies, noting that lower water depths cause an impact on radar sea surface echoes, increase second-order spectral energy, and decrease the saturation limit on wave heights [6,44].

The extreme events analysis shows a seasonal distribution of the events related to the climatic year with two characteristics: the storm season (autumn and winter) and the calm season (spring and summer). Storm activity can be found in the spring period, although it is normally restricted to low-energy events. The class I and class II storms are present throughout the year, although with higher frequencies in autumn/ winter. The storms belonging to the most energetic classes (III, IV and V) mainly occur from October to January, and they are frequently associated with the presence of low-pressure systems over the Tyrrhenian Sea.

Data on the storms selected for this study were retrieved by all three stations of the network, with a delay of the innermost stations of the GoN compared to the external one and with the associated E generally of a lower class (Table 2). At the PORT and CAST sites, the storms typically fall in classes I–III, while only SORR records class IV (and one class V) events. This emphasizes the benefits of covering a given basin with more HFr systems, revealing the specific responses of each sub-basin, as already noted in previous works [9,11,19].

The comparison with model data during storm events typically shows a slight overestimation in Hs_{HF} measurements for the SORR site, while at CAST and PORT an overestimation of the model is reported. Notwithstanding these site-specific issues, it is worth underlining a coherent pattern between the Hs_{HF} and Hs_m data for all the sites investigated. Such discrepancies were already noted in [19], supposedly caused by the inversion method used in HFr data based on an ideal Pierson–Moskovitz spectrum. More thematic investigations are needed to delve into this issue. The implementation of inversion models based on neural networks [73] and of the listen-before-talk operation mode in SeaSonde systems [74] may contribute to more accurate measurements of oceanographic parameters by HFrs.

In addition, it is to be noted that at SORR, where the most energetic events are recorded, Hs_{HF} can reach values greater than 4.0 m, the theoretical higher wave height detectable for a 25 MHz system like the ones operating in the GoN [9]. This evidence does not represent a flaw in the acquisition but rather confirms previous findings [9,11,19], evidencing the ability of HFr to provide reliable measurements even outside a theoretical range in the presence of intense weather conditions.

Radar systems represent an asset of great relevance in the implementation of monitoring networks [64]. HFrs, in particular, have a well demonstrated ability to reconstruct the surface current and wave fields, providing a wealth of information to understand the dynamics of coastal areas [64].

The results gathered in this contribution support the potential of these systems as long-term wave monitoring platforms, and as tools to investigate the characteristics of intense events. Given these outcomes, greater attention might be given in the future to: (i) the study and forecast of storm surges; (ii) the acquisition of wave data from extreme events, improving wave models and integrating coastal altimetry data.

Supplementary Materials: The following supporting information can be downloaded at: https://www.mdpi.com/article/10.3390/rs14071696/s1, Table S1: HFr retrieval at the RC3, RC5 and RC7 at SORR, CAST and PORT from May 2008 to December 2012. Table S2: List of the sea storm events retrieved along the RC3, RC5 and RC7 at SORR, CAST and PORT from May 2008 to December 2012. Figure S1: Density energy spectra evolution (hours with higher values of density energy) during the first event (4 December 2008–7 December 2008) for SORR (first panel), CAST (second panel) and PORT (third panel). Figure S2: Density energy spectra (hours with higher values of density energy) during the second event (1 January 2009–3 January 2009) for SORR (first panel), CAST (second panel) and PORT (third panel). Figure S3: Density energy spectra (hours with higher values of density energy) during the third event (8 November 2010–10 November 2010) for SORR (first panel), CAST (second panel) and PORT (third panel). Figure S4: Density energy spectra (hours with higher values

of density energy) during the third event (28 November 2012–30 November 2012) for SORR (first panel), CAST (second panel) and PORT (third panel).

Author Contributions: Methodology: S.S., D.C. and M.U.; software: S.S. and A.A.B.; validation: S.S., A.A.B., D.C. and M.U.; model data: G.C., L.A.C. and A.P.; data curation: A.A.B. and S.S.; writing—review and editing: S.S., A.A.B., D.C., M.U. and E.Z.; project administration: D.C. All authors have read and agreed to the published version of the manuscript.

Funding: This research was supported by the Project PO FEAMP 2014/2020 (Misura 2.51), funded by Regione Campania (Italy) and partly supported by the 2017 PRIN project EMME (Exploring the fate of Mediterranean microplastic: from distribution pathways to biological effects), funded by the Italian Ministry for Research (grant agreement no. 2017WERYZP).

Institutional Review Board Statement: Not applicable.

Informed Consent Statement: Not applicable.

Data Availability Statement: The data presented in this study are openly available in the links provided in the text.

Acknowledgments: The Department of Science and Technology of the Parthenope University of Naples operates the HF radar system on behalf of the AMRA consortium (formerly CRdC AMRA), a regional competence center for the analysis and monitoring of environmental risks. Our radar remote sites are hosted by the ENEA Centre of Portici, the Villa Angelina Village of High Education and Professional Training and La Villanella resort in Massa Lubrense, and the Fincantieri shipyard in Castellammare di Stabia, whose hospitality is gratefully acknowledged. Mention of trade names or commercial products does not constitute endorsement or recommendation. Technical support by Giovanni Zambardino provided invaluable support to the proper functioning of the HF radar system. The authors thank the Editor and the three anonymous Reviewers for constructive feedback.

Conflicts of Interest: The authors declare no conflict of interest.

References

1. Androulidakis, Y.S.; Kombiadou, K.D.; Makris, C.V.; Baltikas, V.N.; Krestenitis, Y.N. Storm surges in the Mediterranean Sea: Variability and trends under future climatic conditions. *Dyn. Atmos. Ocean.* **2015**, *71*, 56–82. [CrossRef]
2. Martzikos, N.T.; Prinos, P.E.; Memos, C.D.; Tsoukala, V.K. Statistical analysis of Mediterranean coastal storms. *Oceanologia* **2021**, *63*, 133–148. [CrossRef]
3. Conte, D.; Lionello, P. Storm Surge Distribution Along the Mediterranean Coast: Characteristics and Evolution. *Procedia Soc. Behav. Sci.* **2014**, *120*, 110–115. [CrossRef]
4. Vannucchi, V.; Taddei, S.; Capecchi, V.; Bendoni, M.; Brandini, C. Dynamical Downscaling of ERA5 Data on the North-Western Mediterranean Sea: From Atmosphere to High-Resolution Coastal Wave Climate. *J. Mar. Sci. Eng.* **2021**, *9*, 208. [CrossRef]
5. Wyatt, L.R.; Green, J.J.; Middleditch, A. HF radar data quality requirements for wave measurement. *Coast. Eng.* **2011**, *58*, 327–336. [CrossRef]
6. Lipa, B.; Barrick, D.; Alonso-Martirena, A.; Fernandes, M.; Ferrer, M.I.; Nyden, B. Brahan Project High Frequency Radar Ocean Measurements: Currents, Winds, Waves and Their Interactions. *Remote Sens.* **2014**, *6*, 12094–12117. [CrossRef]
7. Lopez, G.; Conley, D.C. Comparison of HF Radar Fields of Directional Wave Spectra Against In Situ Measurements at Multiple Locations. *J. Mar. Sci. Eng.* **2019**, *7*, 271. [CrossRef]
8. Wyatt, L.R. Wave and tidal power measurement using HF radar. *Int. Mar. Energy J.* **2018**, *1*, 123–127. [CrossRef]
9. Saviano, S.; Kalampokis, A.; Zambianchi, E.; Uttieri, M. A year-long assessment of wave measurements retrieved from an HF radar network in the Gulf of Naples (Tyrrhenian Sea, Western Mediterranean Sea). *J. Oper. Oceanogr.* **2019**, *12*, 1–15. [CrossRef]
10. Lorente, P.; Mercader, A.B.; Piedracoba, S.; Perez-Munuzuri, V.; Montero, P.; Sotillo, M.; Álvarez-Fanjul, E. Long-term skill assessment of SeaSonde radar-derived wave parameters in the Galician coast (NW Spain). *Int. J. Remote Sens.* **2019**, *40*, 9208–9236. [CrossRef]
11. Saviano, S.; Cianelli, D.; Zambianchi, E.; Conversano, F.; Uttieri, M. An Integrated Reconstruction of the Multiannual Wave Pattern in the Gulf of Naples (South-Eastern Tyrrhenian Sea, Western Mediterranean Sea). *J. Mar. Sci. Eng.* **2020**, *8*, 372. [CrossRef]
12. Basañez, A.; Lorente, P.; Montero, P.; Álvarez-Fanjul, E.; Pérez-Muñuzuri, V. Quality Assessment and practical interpretation of the wave parameters estimated by HF Radars in NW Spain. *Remote Sens.* **2020**, *12*, 598. [CrossRef]
13. Long, R.M.; Barrick, D.E.; Largier, J.L.; Garfield, N. Wave Observations from Central California: SeaSonde Systems and In SituWave Buoys. *J. Sens.* **2011**, *2011*, 728936. [CrossRef]
14. Alfonso, M.; Álvarez-Fanjul, E.; López, J.D. Comparison of CODAR SeaSonde HF Radar Operational Waves and Currents Measurements with Puertos Del Estado Buoys. Final Report of Puertos del Estado. 2006. Available online: http://www.codar.com/images/about/2006PDE_final_Report.pdf (accessed on 9 January 2021).

15. Bué, I.; Semedo, Á.; Catalão, J. Evaluation of HF Radar Wave Measurements in Iberian Peninsula by Comparison with Satellite Altimetry and in Situ Wave Buoy Observations. *Remote Sens.* **2020**, *12*, 3623. [CrossRef]
16. Orasi, A.; Picone, M.; Drago, A.; Capodici, F.; Gauci, A.; Nardone, G.; Inghilesi, R.; Azzopardi, J.; Galea, A.; Ciraolo, G. Intercomparison of HF radar wave measurements in the Malta-Sicily Channel. In Proceedings of the IMEKO International Conference on Metrology for The Sea, Naples, Italy, 11–13 October 2017.
17. Wyatt, L.R.; Green, J.J.; Gurgel, K.-W.; Borge, J.C.N.; Reichert, K.; Hessner, K.; Günther, H.; Rosenthal, W.; Saetra, O.; Reistad, M. Validation and intercomparisons of wave measurements and models during the EuroROSE experiments. *Coast. Eng.* **2003**, *48*, 1–28. [CrossRef]
18. Bidlot, J.-R.; Holmes, D.J.; Wittmann, P.A.; Lalbeharry, R.; Chen, H.S. Intercomparison of the Performance of Operational Ocean Wave Forecasting Systems with Buoy Data. *Weather Forecast.* **2002**, *17*, 287–310. [CrossRef]
19. Saviano, S.; de Leo, F.; Besio, G.; Zambianchi, E.; Uttieri, M. HF Radar Measurements of Surface Waves in the Gulf of Naples (Southeastern Tyrrhenian Sea): Comparison with Hindcast Results at Different Scales. *Front. Mar. Sci.* **2020**, *7*. [CrossRef]
20. Atan, R.; Goggins, J.; Harnett, M.; Nash, S.; Agostinho, P. Assessment of extreme wave height events in Galway Bay using High Frequency radar (CODAR) data. In *Renewable Energies Offshore*; CRC Press: Boca Raton, FL, USA, 2015; pp. 49–56.
21. Lorente, P.; Sotillo, M.G.; Aouf, L.; Amo-Baladrón, A.; Barrera, E.; Dalphinet, A.; Toledano, C.; Rainaud, R.; de Alfonso, M.; Piedracoba, S.; et al. Extreme Wave Height Events in NW Spain: A Combined Multi-Sensor and Model Approach. *Remote Sens.* **2017**, *10*, 1. [CrossRef]
22. Fernandes, M.; Fernandes, C.; Barroqueiro, T.; Agostinho, P.; Martins, N.; Alonso-Martirena, A. Extreme wave height events in Algarve (Portugal): Comparison between HF radar systems and wave buoys. Proceedings of 5th Jornadas Engenharia Hidrográfica, Lisboa, Portugal, 19–21 June 2018; pp. 222–225.
23. Fortelli, A.; Fedele, A.; de Natale, G.; Matano, F.; Sacchi, M.; Troise, C.; Somma, R. Analysis of Sea Storm Events in the Mediterranean Sea: The Case Study of 28 December 2020 Sea Storm in the Gulf of Naples, Italy. *Appl. Sci.* **2021**, *11*, 11460. [CrossRef]
24. Mendoza, E.T.; Jimenez, J.A.; Mateo, J. A coastal storms intensity scale for the Catalan sea (NW Mediterranean). *Nat. Hazards Earth Syst. Sci.* **2011**, *11*, 2453–2462. [CrossRef]
25. Harley, M. Coastal Storm Definition. In *Coastal Storms*; Wiley: Hoboken, NJ, USA, 2017; pp. 1–21.
26. Dissanayake, P.; Brown, J.; Wisse, P.; Karunarathna, H. Effects of storm clustering on beach/dune evolution. *Mar. Geol.* **2015**, *370*, 63–75. [CrossRef]
27. Lin-Ye, J.; Garcia-Leon, M.; Gracia, V.; Sanchez-Arcilla, A. A multivariate statistical model of extreme events: An application to the Catalan coast. *Coast. Eng.* **2016**, *117*, 138–156. [CrossRef]
28. Morucci, S.; Picone, M.; Nardone, G.; Arena, G. Tides and waves in the Central Mediterranean Sea. *J. Oper. Oceanogr.* **2016**, *9*, s10–s17. [CrossRef]
29. Cianelli, D.; Uttieri, M.; Buonocore, B.; Falco, P.; Zambardino, G.; Zambianchi, E. Dynamics of a Very Special Mediterranean Coastal Area: The Gulf of Naples. In *Mediterranean Ecosystems: Dynamics, Management and Conservation*; Williams, G., Ed.; Nova Science Publishers: New York, NY, USA, 2012; pp. 129–150.
30. Donatini, L.; Lupieri, G.; Contento, G.; Feudale, L.; Pedroncini, A.; Cusati, L.A.; Crosta, A. A high resolution wind&wave forecast model chain for the Mediterranean and Adriatic Sea. In *Towards Green Marine Technology and Transport: Proceedings of the 16th International Conference of the International Maritime Association of the Mediterranean (IMAM2015), Pula, Croatia, 21–24 September 2015*; Guedes Soares, C., Dejhalla, R., Pavletic, D., Eds.; University of Trieste: Trieste, Italy, 2015; Volume 1, pp. 859–866.
31. Ascione, A.; Aucelli, P.P.; Cinque, A.; Di Paola, G.; Mattei, G.; Ruello, M.; Ermolli, E.R.; Santangelo, N.; Valente, E. Geomorphology of Naples and the Campi Flegrei: Human and natural landscapes in a restless land. *J. Maps* **2020**, *17*, 18–28. [CrossRef]
32. Aiello, G.; Caccavale, M. From Siliciclastic to Bioclastic Deposits in the Gulf of Naples: New Highlights from Offshore Ischia and Procida–Pozzuoli Based on Sedimentological and Seismo-Stratigraphic Data. *Quaternary* **2021**, *4*, 44. [CrossRef]
33. Mattei, G.; Di Luccio, D.; Benassai, G.; Anfuso, G.; Budillon, G.; Aucelli, P. Characteristics and coastal effects of a destructive marine storm in the Gulf of Naples (southern Italy). *Nat. Hazards Earth Syst. Sci.* **2021**, *21*, 3809–3825. [CrossRef]
34. Aiello, G.; Sacchi, M. New morpho-bathymetric data on marine hazard in the offshore of Gulf of Naples (Southern Italy). *Nat. Hazards* **2022**, *11*, 2881–2908. [CrossRef]
35. Mattei, G.; Rizzo, A.; Anfuso, G.; Aucelli, P.; Gracia, F. A tool for evaluating the archaeological heritage vulnerability to coastal processes: The case study of Naples Gulf (southern Italy). *Ocean Coast. Manag.* **2019**, *179*. [CrossRef]
36. Falco, P.; Buonocore, B.; Cianelli, D.; de Luca, L.; Giordano, A.; Iermano, I.; Kalampokis, A.; Saviano, S.; Uttieri, M.; Zambardino, G.; et al. Dynamics and sea state in the Gulf of Naples: Potential use of high-frequency radar data in an operational oceanographic context. *J. Oper. Oceanogr.* **2016**, *9*, s33–s45. [CrossRef]
37. Menna, M.; Mercatini, A.; Uttieri, M.; Buonocore, B.; Zambianchi, E. Wintertime transport processes in the Gulf of Naples in-vestigated by HF radar measurements of surface currents. *Nuovo Cimento C* **2007**, *30*, 605–622.
38. Hatzaki, M.; Flocas, H.A.; Simmonds, I.; Kouroutzoglou, J.; Keay, K.; Rudeva, I. Seasonal Aspects of an Objective Climatology of Anticyclones Affecting the Mediterranean. *J. Clim.* **2014**, *27*, 9272–9289. [CrossRef]
39. Amante, C.; Eakins, B.W. *ETOPO1: 1 Arc-Minute Global Relief Model: Procedures, Data Sources and Analysis*; NOAA 595 Technical Memorandum NESDIS NGDC-24; National Geophysical Data Center, NOAA: Boulder, CO, USA, 2009. [CrossRef]

40. Uttieri, M.; Cianelli, D.; Nardelli, B.B.; Buonocore, B.; Falco, P.; Colella, S.; Zambianchi, E. Multiplatform observation of the surface circulation in the Gulf of Naples (Southern Tyrrhenian Sea). *Ocean Dyn.* **2011**, *61*, 779–796. [CrossRef]
41. Cianelli, D.; Falco, P.; Iermano, I.; Mozzillo, P.; Uttieri, M.; Buonocore, B.; Zambardino, G.; Zambianchi, E. Inshore/offshore water exchange in the Gulf of Naples. *J. Mar. Syst.* **2015**, *145*, 37–52. [CrossRef]
42. Cianelli, D.; Uttieri, M.; Guida, R.; Menna, M.; Buonocore, B.; Falco, P.; Zambardino, G.; Zambianchi, E. Land-based remote sensing of coastal basins: Use of a HF radar to investigate surface dynamics and transport processes in the Gulf of Naples. In *Remote Sensing: Techniques, Applications and Technologies*; Alcântara, E., Ed.; Nova Science Publishers: New York, NY, USA, 2013; pp. 1–30. ISBN 9781624171451.
43. Saviano, S.; Esposito, G.; Di Lemma, R.; de Ruggiero, P.; Zambianchi, E.; Pierini, S.; Falco, P.; Buonocore, B.; Cianelli, D.; Uttieri, M. Wind Direction Data from a Coastal HF Radar System in the Gulf of Naples (Central Mediterranean Sea). *Remote Sens.* **2021**, *13*, 1333. [CrossRef]
44. Lipa, B.J.; Nyden, B. Directional wave information from the SeaSonde. *IEEE J. Ocean Eng.* **2005**, *30*, 221–231. [CrossRef]
45. Lipa, B.; Daugharty, M.; Fernandes, M.; Barrick, D.; AlonsoMartirena, A.; Roarty, H.; Dicopoulos, J.; Whelan, C. Developments in compact HF-radar ocean wave measurement. In *Advances in Sensors: Reviews*; Yurish, S.Y., Ed.; IFSA Publishing: Barcelona, Spain, 2018; Volume 5, pp. 469–495.
46. Saha, S.; Moorthi, S.; Pan, H.-L.; Wu, X.; Wang, J.; Nadiga, S.; Tripp, P.; Kistler, R.; Woollen, J.; Behringer, D.; et al. NCEP Climate Forecast System Reanalysis (CFSR) Selected Hourly Time-Series Products, January 1979 to December 2010. *Bull. Am. Meteorol. Soc.* **2010**, *91*, 1015–1058. [CrossRef]
47. Skamarock, W.C.; Klemp, J.B. A time-split nonhydrostatic atmospheric model for weather research and forecasting applications. *J. Comput. Phys.* **2008**, *227*, 3465–3485. [CrossRef]
48. Michalakes, J.; Chen, S.; Dudhia, J.; Hart, L.; Klemp, J.; Middlecoff, J.; Skamarock, W. Development of a Next Generation Regional Weather Research and Forecast Model. Developments in Teracomputing. In *Developments in Teracomputing: Proceedings of the 9th ECMWF Workshop on the Use of High Performance Computing in Meteorology*; Reading, UK, 13–17 November 2000, Zwieflhofer, W., Kreitz, N., Eds.; World Scientific: Singapore, 2001; pp. 269–276.
49. Sorensen, O.R.; Kofoed-Hansen, H.; Rugbjerg, M.; Sorensen, L.S. A Third Generation Spectral Wave Model Using an Unstructured Finite Volume Technique. In Proceedings of the 29th International Conference of Coastal Engineering, Lisbon, Portugal, 19–24 September 2004.
50. Anton, I.A.; Rusu, L. Nearshore Wave Dynamics at Mangalia Beach Simulated by Spectral Models. *J. Mar. Sci. Eng.* **2019**, *7*, 206. [CrossRef]
51. Fonseca, R.B.; Gonçalves, M.; Guedes Soares, C. Comparing the Performance of Spectral Wave Models for Coastal Areas. *J. Coast. Res.* **2017**, *33*, 331–346. [CrossRef]
52. DHI. *MIKE 21 SW Spectral Waves FM Module User Guide*; DHI: Copenhagen, Denmark, 2012.
53. Komen, G.J.; Cavaleri, L.; Doneland, M.; Hasselmann, K.; Hasselmann, S.; Janssen, P.A.E.M. *Dynamics and Modelling of Ocean Waves*; Cambrigde University Press: Cambridge, UK, 1994; p. 554.
54. Young, I.R. Wind generated ocean waves. In *Elsevier Ocean Engineering Book Series, Volume 2*; Bhattacharyya, R., McCormick, M.E., Eds.; Elsevier: Amsterdam, The Netherlands, 1999.
55. Skamarock, W.C.; Klemp, J.B.; Dudhia, J.; Gill, D.O.; Liu, Z.; Berner, J.; Wang, W.; Powers, J.G.; Duda, M.G.; Barker, D.M.; et al. *A Description of the Advanced Research WRF Version 4 NCAR Tech, Note NCAR/TN-556+STR*; National Center for Atmospheric Research: Boulder, CO, USA, 2019; p. 145.
56. Beuvier, J.; Lebeaupin Brossier, C.; Béranger, K.; Arsouze, T.; Bourdallé-Badie, R.; Deltel, C.; Somot, S. MED12, oceanic component for the modeling of the regional Mediterranean Earth System. *Mercator Ocean. Q. Newsl.* **2012**, *46*, 60–66.
57. Wiehle, S.; Pleskachevsky, A. Bathymetry derived from sentinel-1 synthetic aperture radar data. In Proceedings of the EUSAR 2018, 12th European Conference on Synthetic Aperture Radar, Aachen, Germany, 4–7 June 2018; VDE: Frankfurt am Mein, Germany, 2018; pp. 1–4.
58. Lavidas, G.; Venugopal, V. Application of numerical wave models at European coastlines: A review. *Renew. Sustain. Energy Rev.* **2018**, *92*, 489–500. [CrossRef]
59. Hanna, S.; Heinold, D. *Development and Application of a Simple Method for Evaluating Air Quality*; Technical Report; American Petroleum Institute, Health and Environmental Affairs Department: Washington, DC, USA, 1985.
60. Mentaschi, L.; Besio, G.; Cassola, F.; Mazzino, A. Problems in RMSE-based wave model validations. *Ocean Model.* **2013**, *72*, 53–58. [CrossRef]
61. De Swart, R.; Ribas, F.; Calvete, D.; Kroon, A.; Orfila, A. Optimal estimations of directional wave conditions for nearshore field studies. *Cont. Shelf Res.* **2020**, *196*, 104071. [CrossRef]
62. Roarty, H.; Cook, T.; Hazard, L.; George, D.; Harlan, J.; Cosoli, S.; Wyatt, L.; Alvarez Fanjul, E.; Terrill, E.; Otero, M.; et al. The Global High Frequency Radar Network. *Front. Mar. Sci.* **2019**, *6*, 164. [CrossRef]
63. Rubio, A.; Mader, J.; Corgnati, L.; Mantovani, C.; Griffa, A.; Novellino, A.; Quentin, C.; Wyatt, L.; Schulz-Stellenfleth, J.; Horstmann, J.; et al. HF Radar Activity in European Coastal Seas: Next Steps toward a Pan-European HF Radar Network. *Front. Mar. Sci.* **2017**, *4*, 8. [CrossRef]
64. Ludeno, G.; Uttieri, M. Editorial for Special Issue "Radar Technology for Coastal Areas and Open Sea Monitoring. " *J. Mar. Sci. Eng.* **2020**, *8*, 560. [CrossRef]

65. Lopez, G.; Conley, D.C.; Greaves, D. Calibration, Validation, and Analysis of an Empirical Algorithm for the Retrieval of Wave Spectra from HF Radar Sea Echo. *J. Atmos. Ocean. Technol.* **2016**, *33*, 245–261. [CrossRef]
66. Roarty, H.; Evans, C.; Glenn, S.; Zhou, H. Evaluation of algorithms for wave height measurements with High Frequency Ra-dar. In Proceedings of the IEEE/OES Current, Waves and Turbulence Measurements (CWTM), St. Peterburg, FL, USA, 2–6 March 2015; pp. 1–4.
67. Piscopo, V.; Rossi, G.B.; Crenna, F.; Gaglione, S.; Scamardella, A.; Uttieri, M.; Zambianchi, E. Measurement of Sea Waves. In *Measurement for the Sea*; Springer: Berlin/Heidelberg, Germany, 2022; pp. 157–179.
68. Ferla, M.; Nardone, G.; Orasi, A.; Picone, M.; Falco, P.; Zambianchi, E. Sea Monitoring Networks. In *Measurement for the Sea*; Springer Science and Business Media LLC: Berlin/Heidelberg, Germany, 2022; pp. 211–235.
69. Rossi, G.B.; Cannata, A.; Iengo, A.; Migliaccio, M.; Nardone, G.; Piscopo, V.; Zambianchi, E. Measurement of Sea Waves. *Sensors* **2021**, *22*, 78. [CrossRef]
70. Lorente, P.; Lin-Ye, J.; García-León, M.; Reyes, E.; Fernandes, M.; Sotillo, M.G.; Espino, M.; Ruiz, M.I.; Gracia, V.; Perez, S.; et al. On the Performance of High Frequency Radar in the Western Mediterranean During the Record-Breaking Storm Gloria. *Front. Mar. Sci.* **2021**, *8*, 205. [CrossRef]
71. Hernandez-Lasheras, J.; Mourre, B.; Orfila, A.; Santana, A.; Reyes, E.; Tintoré, J. Evaluating high-frequency radar data assimilation impact in coastal ocean operational modelling. *Ocean Sci.* **2021**, *17*, 1157–1175. [CrossRef]
72. Waters, J.; Wyatt, L.R.; Wolf, J.; Hines, A. Data assimilation of partitioned HF radar wave data into Wavewatch III. *Ocean Model.* **2013**, *72*, 17–31. [CrossRef]
73. Hardman, R.L.; Wyatt, L.R. Inversion of HF Radar Doppler Spectra Using a Neural Network. *J. Mar. Sci. Eng.* **2019**, *7*, 255. [CrossRef]
74. Cosoli, S. Implementation of the Listen-Before-Talk Mode for SeaSonde High-Frequency Ocean Radars. *J. Mar. Sci. Eng.* **2020**, *8*, 57. [CrossRef]